Natural Dyes Adsorbed on TiO₂ Nanowire for Photovoltaic Applications: Enhanced Light Absorption and Ultrafast Electron Injection

Sheng Meng, Jun Ren, and Efthimios Kaxiras*

Department of Physics and School of Engineering and Applied Sciences, Harvard University, Cambridge, Massachusetts 02138

ABSTRACT

We investigate the electronic coupling between a TiO₂ nanowire and a natural dye sensitizer, using state-of-the-art time-dependent first-principles calculations. The model dye molecule, cyanidin, is deprotonated into the quinonoidal form upon adsorption on the wire surface. This results in its highest occupied molecular orbital (HOMO) being located in the middle of the TiO₂ bandgap and its lowest unoccupied molecular orbital (LUMO) being close to the TiO₂ conduction band minimum (CBM), leading to greatly enhanced visible light absorption with two prominent peaks at 480 and 650 nm. We find that excited electrons are injected into the TiO₂ conduction band within a time scale of 50 fs with negligible electron–hole recombination and energy dissipation, even though the dye LUMO is located 0.1–0.3 eV lower than the CBM of the TiO₂ nanowire.

The dye-sensitized solar cell (DSSC), often called the "Gratzel cell"[1] after its inventor, is a promising route toward harvesting solar energy in the effort to address the daunting global energy and environment challenges of the 21st century. Since 1991, it has attracted extensive attention from both fundamental and practical perspectives.[2-12] The central idea is to separate the light absorption process from the charge collection process, mimicking natural light harvesting procedures in photosynthesis, by combining dye sensitizers with semiconductors. This enables the use of widegap but cheap oxide semiconductors such as TiO₂. To be effective, it requires the highest occupied molecular orbital (HOMO) of the dye to reside in the bandgap of the semiconductor and its lowest unoccupied molecular orbital (LUMO) to lie within the conduction band of the semiconductor.[8] The efficiency is determined by two main factors: (i) the maximum photocurrent density, I_{ph}, related to the charge injection rate from the dye HOMO to the semiconductor conduction bands and (ii) the open circuit potential, V_{oc}, related to the energy difference between the HOMO and the conduction band minimum (CBM). Consequently, the DSSC has advantages in both low-cost and high-efficiency,[3] relative to the more established technologies based on monocrystalline Si and nanocrystalline thin-film solar cells.[14]

Early DSSC designs involved transition metal coordinated compounds (e.g., ruthenium polypyridyl complexes) as sensitizers because of their strong visible absorption, long excitation lifetime, and efficient metal-to-ligand charge transfer.[1,5-8] Although highly effective, with current maximum efficiency of 11%,[3] the costly synthesis and undesired environmental impact of those prototypes call for cheaper, simpler, and safer dyes as alternatives.[9] Natural pigments, including chlorophyll, carotene, and cyanin,[9-12] are freely available in plant leaves, flowers, and fruits and fulfill these requirements. Experimentally, natural-dye sensitized TiO₂ solar cells have reached an efficiency of 7.1% and high stability.[12] Higher efficiency over 8.0% has been obtained using similar synthetic organic dyes.[13]

Recent efforts to develop DSSCs have also made use of one-dimensional (1D) nanowire [4,5] and nanotube [6,7] structures of semiconductors. Compared to the commonly used nanoparticles, 1D nanowires (including nanotubes) provide additional benefits in two respects: (i) due to their high length-to-diameter ratio and a total length reaching hundreds of micrometers, visible light scattering and absorption are much enhanced in nanowires; (ii) the 1D geometry facilitates rapid, diffusion-free electron transport to the electrodes. Both effects have been verified in experiments.[5,7]

Despite intensive experimental and theoretical studies on surface-based (2D)[15-17] and nanoparticle-based (0D)[8,18-20] DSSCs, the mechanism and electronic coupling between a TiO₂ nanowire and a dye molecule, especially a natural one, has never been addressed. The goal of the present work is to elucidate the coupling between a TiO₂ nanowire and natural dyes and to provide insight into charge injection mechanisms of natural-dye sensitized nanowire solar cells.

In particular, our extensive calculations, based on time-dependent density functional theory (TDDFT),[21] show that electrons can be injected from cyanin dyes to the TiO$_2$ nanowire within 50 fs after excitation, although the dye LUMO is lower than the TiO$_2$ CBM by 0.1–0.3 eV. This extends the current understanding of the mechanisms of DSSC operation and thus can enhance the ability to optimize their design and efficiency.

The first-principles density functional theory (DFT) calculations were carried out with the SIESTA code.[22] We use pseudopotentials of the Troullier–Martins type[23] to model the atomic cores, the PBE form of the exchange-correlation functional,[24] and a local basis set of double-ζ polarized orbitals (19 numerical atomic orbitals for Ti including semicore 3 s and 3 p states;[25] 13 orbitals for C, N, and O; 5 orbitals for H). An auxiliary real space grid equivalent to a plane-wave cutoff of 70 Ry is used for the calculation of the electrostatic (Hartree) term. Solvent molecules are not included in our model structures, since they usually participate only in weak interactions such as hydrogen bonding; their influences are subject to future investigations. The optical absorption spectra and coupled electron–ion dynamics of the dye–TiO$_2$ system are extracted from TDDFT simulations. Optical absorbance is calculated within the linear response regime,[26] by propagating the wave functions 6107 steps in time with a time step of 0.0034 fs, which gives an energy resolution of 0.1 eV. The perturbing external electric field is 0.1 V/Å. This computational scheme gives optical absorption spectra that are in good agreement with experiment for a range of biologically relevant molecules such as DNA bases,[26] with a typical accuracy of 0.2–0.3 eV. For the simulation of electron injection, the evolution of both electrons and ions in real time is monitored after excitation. The time-dependent Kohn–Sham equations of electrons and the Newtonian motion of ions are solved simultaneously, with ionic forces along the classical trajectory evaluated through the Ehrenfest theorem. The electron density is updated self-consistently during the real-time propagation of single-particle Kohn–Sham wave functions with a time step of 0.02419 fs. The initial velocity of ions is assigned according to the equilibrium Boltzmann–Maxwell distribution at a given temperature. Within this scheme, the total energy is well conserved to within 10^{-4} eV/fs. This convergence is by choice; better performance can be obtained if a more stringent criterion for each step is chosen. In practice, we have checked that such a convergence produces negligible differences in energy levels evolution and electron–ion dynamics. The use of TDDFT for treating excited states and dynamics has been debated recently,[27,28] and the latest results have shown it to be accurate in many applications.[29] This scheme reproduces successfully experimental parameters of small molecules in excited states as well as in the ground state; for example, for the CO excited state, we calculate a bond length of 1.24 Å and vibrational frequency of 1689 cm^{-1} which compare well with the experimental values[30] of 1.24 Å and 1518 cm^{-1} [the ground-state calculated values are 1.15 Å and 2245 cm^{-1}, and the experimental ones,[30] 1.13 Å and 2170 cm^{-1}].
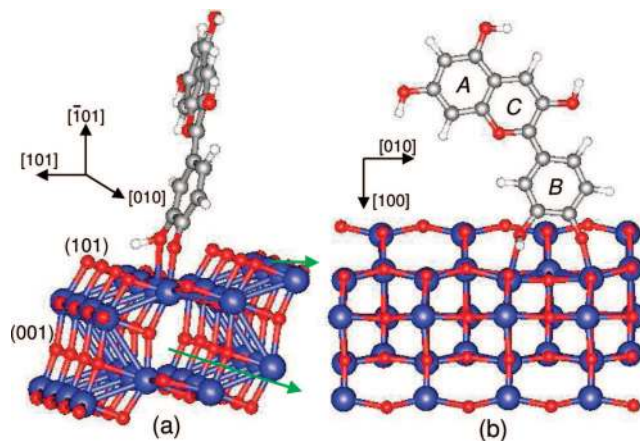
Figure 1. Unit cell for a prototypical TiO$_2$ nanowire sensitized by the cyanidin dye: (a) side view; (b) top view. Ti, O, C, and H atoms are represented by blue, red, gray, and white spheres, respectively. Green arrows indicate two possible nanowire axis directions.

We use the anatase phase of TiO$_2$ to construct model TiO$_2$ nanowires. This phase is found to be active in light absorption and photon-to-current conversion and is the prevalent one in experiments.[31] The experimental lattice constants of $a = b = 3.784$ Å and $c = 9.515$ Å are employed, which are close to the theoretical values of 3.80 and 9.53 Å. Figure 1 shows a segment of TiO$_2$ nanowire comprising 32 TiO$_2$ units in the anatase phase. This segment exposes four (101) and two (001) facets. Both surfaces are stable, with the former being more favorable, as observed in monocrystals and nanoparticles.[3] In principle, the nanowire unit can be repeated along either the [010] or the [101] direction, forming two nanowire structures of different orientation. The latter structure is similar to that repeated along the [1$\bar{1}$1] direction, with all facets being (101). We studied all these structures and focused on wires along the [010] and [1$\bar{1}$1] directions, to which we refer according to their axial direction, [010]-wire and [1$\bar{1}$1]-wire. Periodic boundary conditions are used in the directions perpendicular to the wire axis, which separate the nanowire from its images by at least 10 Å of vacuum. We note that the nanowire structures constructed here are smaller than those used in experiment, whose diameter is typically 30–80 nm (wall thickness ~8–20 nm for nanotubes).[5–7] However, our structures have other features (e.g., 1D geometry, orientation, and facets) which are the same as experimental ones and thus represent a reasonable model.

For the dye molecule, we chose cyanin as a prototype because of its simple structure and easy purification as compared to the other two abundant natural pigments, chlorophyll and carotene. Another useful property of cyanin is its strong visible absorption around 520 nm in solution.[9] Cyanin is a flavonoid molecule comprising two aromatic rings (A and B), and an oxygenated heterocyclic ring (C) which attaches to a sugar moiety. As the sugar group has a bandgap >5.7 eV, it does not contribute to absorption at wavelengths λ > 210 nm. Therefore we consider only the base structure of cyanin without the sugar group, the cyanidin (Cya) molecule. A representative structure for a Cya adsorbed on the TiO$_2$ nanowire is shown in Figure 1a and 1b. The
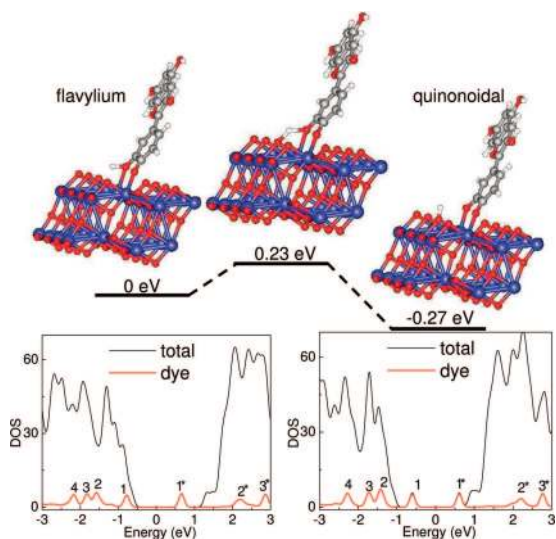
Figure 2. Deprotonation pathway and energy profile for a cyanidin adsorbed on the TiO₂ nanowire with the axis along the [010] direction (the [010]-wire). Total density of states (DOS) (thin black line) and that projected on the dye molecule (thick red line) are shown for structures before and after the deprotonation. States from the dye molecule are numbered as 1, 2, 3,... for occupied states counting from the HOMO toward lower energies, and 1*, 2*, 3*,... for unoccupied states counting from the LUMO toward higher energies. The Fermi level is set to zero.

corresponding surface coverage is 1 cyanidin molecule per 153 Å², namely, 1 μmol·m⁻².

We first consider cyanidin adsorption on the [010]-wire. We explore the possibility of adsorption on different facets and several sites; from this study, we determined that adsorption onto neighboring Ti ions of the (101) facet along [010] through the carbonyl and hydroxyl groups of ring-*B* is the most stable. Furthermore, our calculations reveal that upon adsorption Cya transfers the H of the hydroxyl group to the nanowire and is deprotonated. Figure 2 shows the deprotonation pathway and the corresponding electronic structures of initial and final states. Initially, Cya adsorbs intact in the flavylium form, with its OH on ring-*B* pointing to the oxygen atom of the wire forming a hydrogen bond. The OH covalent bond and hydrogen bond lengths are 1.04 and 1.51 Å, respectively. The Ti–O bond length formed between the nanowire and the hydroxyl (carbonyl) group is 2.23 Å (1.93 Å). In the transition state, the hydroxyl H atom forms two intermediate bonds with O atoms from Cya and TiO₂, the corresponding OH distances being almost identical, 1.31 and 1.28 Å, respectively. The total energy increases by 0.23 eV compared to the initial state, indicating a small barrier of 0.23 eV for the H transfer process. After that, the H is completely transferred to the surface O of TiO₂ with a bond length of 1.02 Å. The Cya molecule anchors itself on the neighboring O atoms along the [010] direction of the nanowire with Ti–O bond lengths of 1.97 and 1.91 Å, forming the quinonoidal form. The deprotonation process lowers the system energy by 0.27 eV, resulting in a Cya binding energy of 1.0 eV on the TiO₂ nanowire with respect to a free Cya molecule and a bare nanowire.

The total density of states (DOS) and that projected on Cya are shown for the dye/wire system before and after

deprotonation. Overall, the DOS of the TiO₂ nanowire is similar to that for bulk TiO₂. The occupied orbitals of Cya are labeled as 1, 2, 3,... counting from the HOMO toward lower energies and the unoccupied orbitals as 1*, 2*, 3*,... counting from the LUMO to higher energies. Before deprotonation, the Cya HOMO lies within the valence band (VB) of TiO₂ while the LUMO is far from the CBM of TiO₂ (the latter being higher by 0.7 eV); both are unfavorable for charge injection. After deprotonation, however, the HOMO is shifted into the bandgap region of TiO₂ and the LUMO moves toward the CBM of TiO₂, which is now higher by only 0.3 eV. This is critical for solar cell applications, because in such cases excitation from the dye HOMO to the conduction band of TiO₂ is much easier than from the TiO₂ VB and involves visible light, given the smaller bandgap of isolated cyanidin (2.4 eV) compared to that of anatase TiO₂ (3.2−3.3 eV).[18] Our finding is consistent with the experimental observation[9] that upon Cya adsorption the color of the solution changes from red (flavylium) to purple (quinonoidal), indicating that depronation takes place. Deprotonation of Ru-complex dyes attached to TiO₂ nanoparticles was found to be responsible for the strong dye/TiO₂ coupling recently.[18]

This behavior is quite general for other dye/wire configurations. Deprotonation of Cya results in favorable overlap of the dye orbitals and the TiO₂ bandgap, though the HOMO and LUMO positions may vary from case to case. For example, the LUMO is 0.42 eV lower than the CBM of TiO₂ for Cya attached on the edge of the (101) facet and 0.48 eV lower for Cya attached on the (001) facet, while the HOMO−LUMO difference is almost constant. These structures are 0.4 and 0.1 eV less stable than that shown in Figure 2. We also studied configurations with the proton transferred to different TiO₂ sites, which are typically less stable by 0.2 eV.

The same is true for other wire orientations as well. The [101]-wire and the [1̄11]-wire are more stable than the [010]-wire by 0.26 and 0.27 eV per TiO₂ unit, respectively, because their facets are more stable (101) faces. The Cya LUMO is 0.27 and 0.20 eV lower than the CBM of TiO₂ after deprotonation on these two wires, respectively, resulting in Cya adsorption energies around 1.5 eV. The latter structure with dye adsorption is shown in Figure 3a. From the corresponding DOS plot, the LUMO of Cya is almost degenerate with the CBM of TiO₂ (Figure 3b). The wave functions of the states labeled 1 (HOMO), 1* (LUMO), and CBM (LUMO + 1) at the Γ k-point are shown in Figure 3c−e. In the HOMO and LUMO states, electrons are mainly localized in the Cya molecule, with a small fraction transferred to Ti ions. The main difference is the bonding and antibonding character between ring-*B* and ring-*C* for the HOMO and LUMO, respectively. In the LUMO + 1 state, electrons are delocalized and distributed in the whole nanowire, mainly in Ti d$_{xy}$ orbitals. Detailed analysis of this state reveals that 88% of electrons reside on the Ti orbitals, which is the CBM of the TiO₂ nanowire. We conclude from this analysis that an incident photon absorbed by Cya will promote an electron from its HOMO to its LUMO state, then
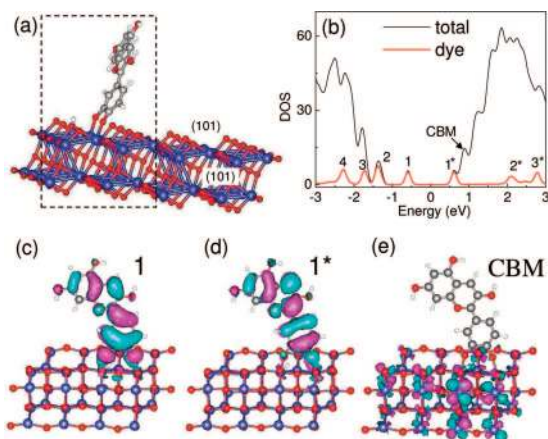
Figure 3. (a) Structure of the dye-sensitized TiO$_2$ [1$\bar{1}$1]-wire with all facets being (101). Dashed lines mark the unit cell in the calculation. (b) Total (thin black line) and projected (thick red line) density of states for this system. The corresponding wave functions for the (c) HOMO, (d) LUMO, and (e) LUMO + 1 states at the Γ k-point.

Figure 4. Optical absorption spectra of a finite segment of TiO$_2$ nanowire (inset) with (solid) and without (dashed) sensitizing dye molecules. The calculated spectrum for a free cyanidin molecule is also shown (dotted), together with the experimental peak position (vertical bar).

the electron will be injected into the conduction band of the TiO$_2$ nanowire.

We have also investigated the dependence of the LUMO−CBM energy difference on the size of the nanowire. The [1$\bar{1}$1]-wire of width 2 units, 4 units, and infinity (that is, the 2D (101) surface) have LUMO−CBM separations of 0.38, 0.20, and 0.09 eV, respectively. Therefore, we expect that the larger dimensions of the nanowire used in experiment will result in smaller energy separation (∼0.1 eV) between the LUMO and the CBM of TiO$_2$ than what we showed here for small model nanowires. In addition, we have also considered TiO$_2$ nanowire structures with O vacancy defects, which are dominant on TiO$_2$ surfaces. Three different types of O vacancy were analyzed. The first type involves the O vacancy located at one of the four edges of the wire; the second type involves an O vacancy on the surface steps, that is, the outermost oxygen rows, which connect the 5-fold and 6-fold Ti ions of the wire; the third type of O vacancy lies in the flat surface terrace, the oxygen that connects two 5-fold Ti ions. All three types are possible, with the energy difference between them less than 0.1 eV per vacancy. Not surprisingly, the O vacancy right beneath the Cya molecule enhances dye adsorption significantly (adsorption energy 2.7 eV) and results in the LUMO being slightly higher in energy than the CBM of TiO$_2$, by 0.16 eV.

We calculated the optical properties of the Cya/TiO$_2$ nanowire using TDDFT. The commonly used local and semilocal approximations for the exchange-correlation function typically employed in these calculations lack the correct −1/r asymptotic behavior,[27,29] where r is the distance between the hole and the electron. As a consequence, in infinitely long (periodic) structures, the results of TDDFT calculations suffer from the same limitations as regular DFT calculations in reproducing the energies of excited states. To avoid this problem, we used a finite segment of the nanowire. The [1$\bar{1}$1]-nanowire with a narrow width (2 repeat units) is terminated by OH or H at the two ends along its axis, resulting in a structure consisting of 20(TiO$_2$)·2(H$_2$O), shown
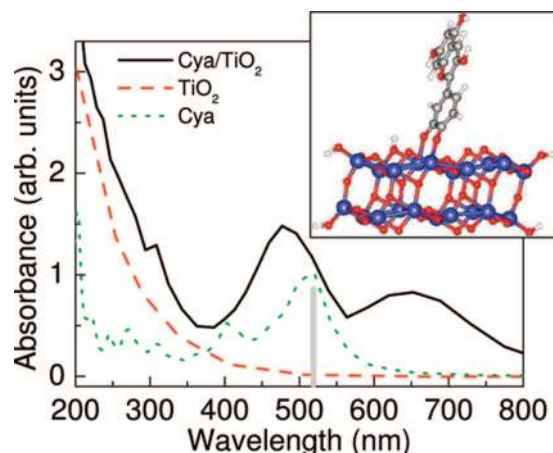
in Figure 4 (inset). We checked that this finite structure reproduces well the DOS features of the infinite nanowire. The optical absorption of the dye/wire structure is shown in Figure 4. For comparison, we also calculated absorption spectra for the bare TiO$_2$ nanowire and free Cya molecules. Cya exhibits two major absorption bands at 520 and 410 nm, respectively. These peaks are prominent and red-shifted to 650 and 480 nm for Cya adsorbed on the TiO$_2$ nanowire, with intensity much enhanced due to the interfacial Ti−O coupling between the molecule and the wire. These peaks correspond to excitations from state 1 (HOMO) and state 2 (HOMO − 1) to state 1* (LUMO) as labeled in Figure 3. The red-shift is also consistent with the decreased bandgap of the adsorbed Cya (1.15 eV) compared to that of free Cya (1.45 eV) in DFT calculations. Direct excitation from Cya orbitals to the TiO$_2$ conduction band is less important, as verified by the negligible transition dipole moment between them. On the other hand, the bare TiO$_2$ nanowire shows no absorption beyond 400 nm, consistent with its large bandgap ∼3.2 eV.[18] Therefore, the dye sensitizer greatly increases the absorption of the TiO$_2$ nanowire in the visible range, which dominates the terrestrial solar spectrum. Comparing with experiment, free cyanin solution and cyanin on TiO$_2$ nanoparticles[9] show absorption peaks at 520 and 532 nm, respectively, and the latter exhibits two major emission peaks at 550 and 740 nm, consistent with our results. In addition, rosella extract with the main component being cyanin shows a strong absorption peak at 560 nm and a shoulder at 650 nm after adsorption on TiO$_2$ nanoparticles,[11] which agrees well with our calculated spectrum. The differences may be assigned to the versatility of dye adsorption configurations and different TiO$_2$ structures (nanowires in the calculation versus nanoparticles in experiment).

In order to make solar cells efficient, rapid charge injection and transport are required in addition to intense visible light absorption. Many previous studies have emphasized that the dye LUMO being higher than the CBM of TiO$_2$ is beneficial for efficient electron injection.[8,17,19] However, this causes

other problems for DSSCs, namely, the electrons excited to the dye LUMO can dissipate through nonradiative processes into the lower-lying CBM of TiO$_2$, reducing significantly the open circuit potential V_{oc} and causing unwanted energy loss.[8,32] The ideal case would be that the LUMO is close to and slightly higher than the CBM to produce both large V_{oc} and high injection rates, ultimately leading to large I_{ph} accompanied by intense light absorption. For our system of natural-dye sensitized TiO$_2$ nanowire, large V_{oc} would not be a limitation because of the large difference between the HOMO and CBM. We demonstrate below that this structure also facilitates ultrafast electron injection from the dye LUMO to the CBM of the TiO$_2$ wire, a result coming from their close match in energy, despite the fact that the LUMO is slightly lower.

We monitor the electron injection process from Cya to the TiO$_2$ nanowire under 1D periodic boundary conditions after photon absorption using TDDFT. TDDFT has been used to calculate the lifetime of excited adsorbate states at metal surfaces.[33] Ehrenfest dynamics based on TDDFT has been previously applied to study excited-state dynamics successfully[34−37] though other than surface hopping methods,[16,38] as a mean-field approach it could suffer from problems such as the lack of state-specific information and detailed balance,[39] which are not of interest in the present study. Our TDDFT approach is considerably different from that of Prezhdo and co-workers[15,16] in several aspects: (i) We use very efficient local basis sets, which are small in size and fast in performance, while they use planewaves. (ii) In planewave calculations, periodic boundary conditions have to be invoked, while we could use either periodic or finite-sized supercells by choice. The latter choice, not possible with planewaves, is particularly suitable for low-dimensional nanomaterials, where a large vacuum space is present. (iii) They use ground-state trajectories in their excited-state MD simulations, and the Hamiltonian between two ionic steps is not updated with the evolution of electron density when propagating the one-electron wave functions. In contrast to that approach, we use TDDFT to propagate the many-electron density self-consistently *at every electronic and ionic step*, and use excited-state trajectories with forces calculated from mean-field theory. In this respect, our approach is the first of its kind to tackle the electron−ion dynamics at the dye/TiO2 interface using the full TDDFT treatment.

Figure 5a shows the evolution of electronic energy levels with respect to simulation time. At time $t = 0$, one electron is promoted from the HOMO to the LUMO of Cya, which is a good approximation for representing the first excited state.[35] Electronic state diagonalization is performed at this first step after the occupation switch. We then let the coupled electron−ion system evolve in real time. The initial ionic temperature is set to 350 K. The energy of the LUMO, occupied with one electron after excitation, first approaches that of the CBM of TiO$_2$ and later diverges from it. There is a crossover at time 30 fs, after which the two states seem mixed, evidenced by the large off-diagonal Hamiltonian matrix element (not shown). The density distribution of the excited electron is also monitored and projected onto all Ti
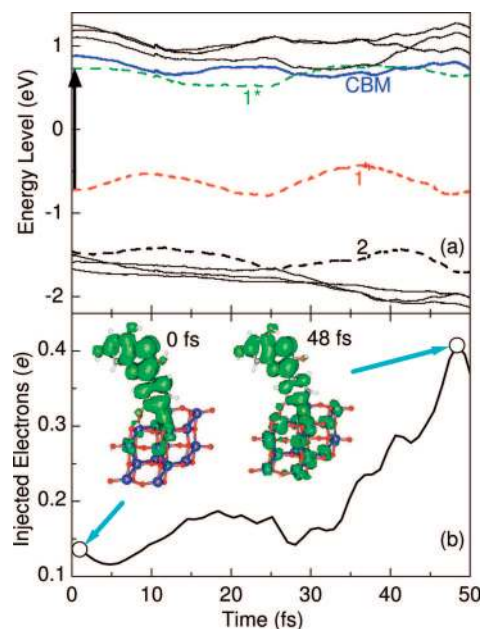
Figure 5. (a) Evolution of electronic state energy levels after excitation of cyanidin from its HOMO (state 1) to the LUMO (state 1*). Energy levels contributed by the dye are shown in dotted lines. (b) Fraction of electrons injected to the TiO$_2$ nanowire as a function of time after excitation. The insets show the charge density of the excited electron at $t = 0$ and 48 fs at the contour level of 0.004 $e/\text{Å}^3$.

and O atomic orbitals in the nanowire. The latter is considered as the "injected" electrons into the nanowire. We found that at $t = 0$ only 0.14 e is distributed on the TiO$_2$, due to the electronic coupling between Cya and the wire through carbonyl groups. This value decreases slightly then starts to increase after 5 fs (Figure 5b). As a result, the injected electrons reach a first maximum of 0.2 e at $t = 18$ fs and a second maximum of 0.4 e at $t = 48$ fs. The value increases further to 0.6 e around $t = 63$ fs (not shown), but our analysis shows that the off-diagonal matrix element between the LUMO and the lowest conduction band becomes large (>0.05 eV, comparable to their separation $\sim 0.06 - 0.10$ eV) after this time, indicating a large probability of state mixing through nonradiative internal conversion. The nonadiabatic transition probability can be estimated through the Landau−Zener formula,[40] which shows large probabilities ($>90\%$) for the electron to transfer from the dye LUMO to the conduction band of the semiconductor during this time (see the Supporting Information). This ultrafast charge injection is more obvious if we compare the density distribution of the excited electron at $t = 0$ and 48 fs in Figure 5b. The electron injection data can be fitted by an exponential decay with a lifetime of 16 fs after a time delay of 33 fs, giving the total time scale ~ 50 fs (see the Supporting Information). On the other hand, direct recombination of the electron and the hole is unfavorable because the off-diagonal matrix element between them is <0.04 eV, much smaller than their large energy separation of 1.40 eV, which gives zero Landau−Zener probabilities (see the Supporting Information), indicating that the lifetime of the excited-state is
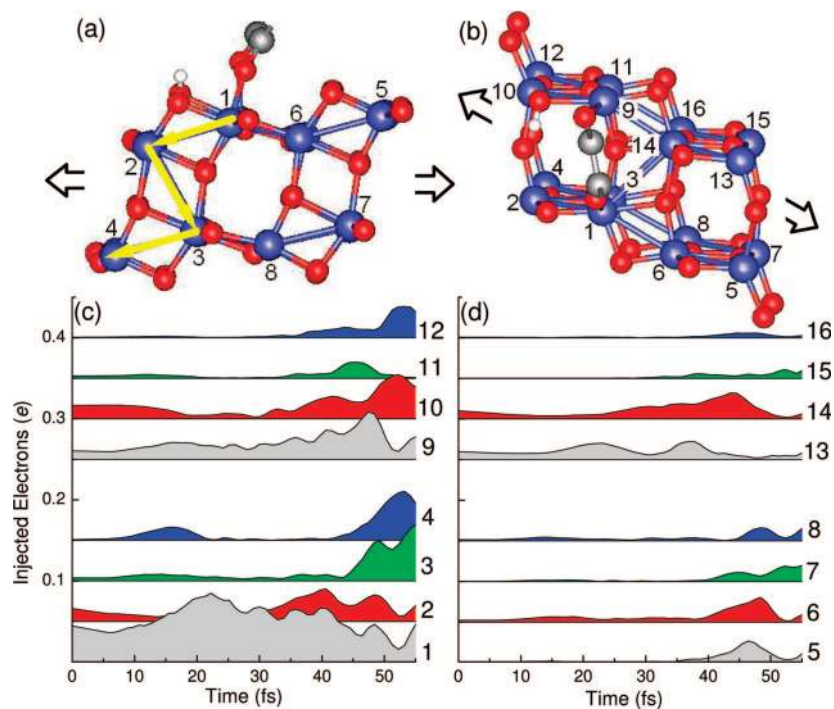
Figure 6. Electron transport pathways inside the nanowire. All Ti ions are numbered explicitly in (a) the side view and (b) the top view. Only the bottom part of the adsorbed cyanidin molecule (O−C−C−O) is shown. Arrows indicate the direction of the nanowire axis. (c−d) Injected electron distribution projected on each Ti in the nanowire unitcell shown as a function of simulation time. For better view, lines are shifted vertically by 0.05 for consecutive curves.

long. Experimental measurements[9] have revealed ultrafast electron injection from cyanin to TiO_2 nanoparticles within less than 100 fs and a recombination lifetime of 67 ps, in good agreement with our result. Later experimental[41,42] and theoretical studies[15,17] confirmed that even faster injection processes, within 10 fs or less, take place from other organic dyes (alizarin, bi-isonicotinic acid, catechol) to TiO_2. We note that the self-interaction energy, which is the source of errors for TDDFT simulations involving charge transfer excitations,[27] is small in the present case. From the energy difference of the same orbital between full and empty occupancy, we estimate that the self-interaction errors for the HOMO and the LUMO are on the order of 0.2 eV. We also note that the charge injection through state-mixing discussed above is *not* a direct charge transfer excitation.

We further analyzed the pathways of the injected electron and its transport inside the nanowire. Figure 6 shows the fraction of electrons projected on each Ti ion of the nanowire during charge injection. Ti ions are numbered explicitly in the unit cell in four rows from top (where Cya sits) to bottom. Not surprisingly, the electron is mainly distributed on Ti1, which is bonded to the carbonyl group on the *B*-ring of Cya, and Ti9, where the deprotonated hydroxyl group binds. From Figure 6a, we find that electrons proceed along Ti1 → Ti2 → Ti3 → Ti4 during charge injection, resulting in density maxima in Ti4 at $t = 16$ and 52 fs. Other pathways following the same direction show approximately the same trend. This indicates that electrons first flow in and fill the whole nanowire. Parallel charge transport along the nanowire axis, such as, Ti1 → Ti6 → Ti5 → Ti2′ (Ti2′ being the image of Ti2 in the next cell) is less favorable, judging by the small

density and the later appearance of electrons in this path. Efficient charge transport could take place along the Ti13 → Ti14 → Ti9 → Ti10 direction at a later time. Interestingly, previous quantum dynamics simulations with a model Hamiltonian have shown[17] that charge injection along the [101] direction is an order of magnitude slower than that along [$\bar{1}$01] for electrons excited to the HOMO of catechol on TiO_2, consistent with our results (note that the direction indices are reversed in ref 17). Therefore, we have demonstrated from first principles that both charge injection and charge transport occur effectively at the ultrafast time scale in the natural-dye sensitized TiO_2 nanowire, even though in this system the dye LUMO is slightly lower than the CBM of the semiconductor, mainly due to the influence of ionic thermal motions in the dye/nanowire system. As a result, both a large V_{oc} and a high electron injection rate can be achieved, which would result in a high efficiency of the natural-dye sensitized TiO_2 nanowire solar cells.

In conclusion, we have investigated the electronic coupling and charge injection process in the natural-dye sensitized TiO_2 nanowire solar cells using cyanidin as a model molecule. Comparing with traditional DSSCs, this system has additional advantages such as free availability of the dye, large surface area, environmentally benign components, and improved light scattering and charge transport, all of which contribute toward improving key charateristics, that is, low cost and high efficiency. Various nanowire orientations and dye adsorption sites were explored, which demonstrate that deprotonation of the dye leads to the HOMO being inside the bandgap and the LUMO very close to the CBM of TiO_2. Oxygen vacancy defects further improve dye adsorption.

Visible light absorption is greatly enhanced due to the presence of the dye molecules. Real-time TDDFT simulations reveal that excited electrons are injected into the conduction band of TiO_2 at the ultrafast time scale of 50 fs, despite the fact that the CBM is 0.1−0.3 eV higher in energy than the dye LUMO. This effect is assigned to the thermal fluctuations of ions. As a result, both high V_{oc} and large I_{ph} could be obtained for this prototypical natural-dye sensitized nanowire cell. Our results agree with available experimental absorption spectra and electron injection kinetics. Further improvements can be achieved by attaching more dye molecules to the facets of the nanowire, forming a high density antenna system similar to natural photosynthesis, which is a unique advantage of the 1D nanowire system. Such investigations are underway.

Supporting Information Available: Estimation of the decay probability during photoexcitation using Landau−Zener formula and the fitting to the electron injection. This material is available free of charge via the Internet at http://pubs.acs.org.

References

(1) O'Regan, B.; Gratzel, M. *Nature* **1991**, *353*, 737–740.

(2) Gratzel, M. *J. Photochem. Photobiol. C* **2003**, *4*, 145–153.

(3) Gratzel, M. *Chem. Lett.* **2005**, *34*, 8–13.

(4) Law, M.; Greene, L. E.; Johnson, J. C.; Saykally, R.; Yang, P. *Nat. Mater.* **2005**, *4*, 455–459.

(5) Tan, B.; Wu, Y. Y. *J. Phys. Chem. B* **2006**, *110*, 15932–15938.

(6) Mor, G. K.; Shankar, K.; Paulose, M.; Varghese, O. K.; Grimes, C. A. *Nano Lett.* **2006**, *6*, 215–218.

(7) Zhu, K.; Neale, N. R.; Miedaner, A.; Frank, A. J. *Nano Lett.* **2007**, *7*, 69–74.

(8) De Angelis, F.; Fantacci, S.; Selloni, A.; Gratzel, M.; Nazeeruddin, M. K. *Nano Lett.* **2007**, *7*, 3189–3195.

(9) Cherepy, N. J.; Smestad, G. P.; Gratzel, M.; Zhang, J. Z. *J. Phys. Chem. B* **1997**, *101*, 9342–9351.

(10) Hao, S.; Wu, J. H.; Huang, Y. F.; Lin, J. M. *Sol. Energy* **2006**, *80*, 209–214.

(11) Wongcharee, K.; Meeyoo, V.; Chavadej, S. *Sol. Energy Mater. Sol. Cells* **2007**, *91*, 566–571.

(12) Chapbell, W. M.; Jolley, K. W.; Wagner, P.; Wagner, K.; Walsh, P. J.; Gordon, K. C.; Schmidt-Mende, L.; Nazeeruddin, M. K.; Wang, Q.; Gratzel, M.; Officer, D. L. *J. Phys. Chem. C* **2007**, *111*, 11760–11762.

(13) Kim, S.; Lee, J. K.; Kang, S. O.; Ko, J.; Yum, J. H.; Fantacci, S.; De Angelis, F.; Di Censo, D.; Nazeeruddin, M. K.; Gratzel, M. *J. Am. Chem. Soc.* **2006**, *128*, 16701–16707.

(14) Lewis, N. S. *Science* **2007**, *315*, 798–801.

(15) Stier, W.; Duncan, W. R.; Prezhdo, O. V. *Adv. Mater.* **2004**, *16*, 240–244.

(16) Duncan, W. R.; Craig, C. F.; Prezhdo, O. V. *J. Am. Chem. Soc.* **2007**, *129*, 8528–8543.

(17) Rego, L. G. C.; Batista, V. S. *J. Am. Chem. Soc.* **2003**, *125*, 7989–7997.

(18) De Angelis, F.; Fantacci, S.; Selloni, A.; Nazeeruddin, M. K.; Gratzel, M. *J. Am. Chem. Soc.* **2007**, *129*, 14156–14157.

(19) Persson, P.; Lundqvist, M. J. *J. Phys. Chem. B* **2005**, *109*, 11918–11924.

(20) Persson, P.; Lundqvist, M. J.; Ernstorfer, R.; Goddard, W. A., III; Willig, F. *J. Chem. Theory Comput.* **2006**, *2*, 441–451.

(21) Runge, E.; Gross, E. K. U. *Phys. Rev. Lett.* **1984**, *52*, 997.

(22) Soler, J. M.; Artacho, E.; Gale, J. D.; Garcia, A.; Junquera, J.; Ordejon, P.; Sanchez-Portal, D. *J. Phys.: Condens. Matter* **2002**, *14*, 2745–2779.

(23) Troullier, N.; Martins, J. L. *Phys. Rev. B* **1991**, *43*, 1993–2006.

(24) Perdew, J. P.; Burke, K.; Ernzerhof, M. *Phys. Rev. Lett.* **1996**, *77*, 3865–3868.

(25) Junquera, J.; Zimmer, M.; Ordejon, P. Ghosez, Ph. *Phys. Rev. B* **2003**, *67*, 155327.

(26) Tsolakidis, A.; Kaxiras, E. *J. Phys. Chem. A* **2005**, *109*, 2373–2380.

(27) Dreuw, A.; Head-Gordon, M. *J. Am. Chem. Soc.* **2004**, *126*, 4007–4016.

(28) Levine, B. G.; Ko, C.; Quenneville, J.; Martinez, T. J. *Mol. Phys.* **2006**, *104*, 1039–1051.

(29) Burke, K.; Werschnik, J.; Gross, E. K. U. *J. Chem. Phys.* **2005**, *123*, 062206.

(30) *NIST Chemistry WebBook, NIST Standard Reference Database 69*; Linstrom, P. J., Mallard, W. G., Eds.; 2005 (http://webbook.nist.gov).

(31) Mor, G. K.; Varghese, O. K.; Paulose, M.; Shankar, K.; Grimes, C. A. *Sol. Energy Mater. Sol. Cells* **2006**, *90*, 2011–2075.

(32) Duncan, W. R.; Prezhdo, O. V. *Annu. Rev. Phys. Chem.* **2007**, *58*, 143–184.

(33) Li, X.; Tully, J. C. *Chem. Phys. Lett.* **2007**, *439*, 199–203.

(34) Castro, A.; Marques, M. A. L.; Alonso, J. A.; Bertsch, G. F.; Rubio, A. *Eur. Phys. J. D* **2004**, *28*, 211–218.

(35) Tavernelli, I.; Rohrig, U. F.; Rothlisberger, U. *Mol. Phys.* **2005**, *103*, 963–981.

(36) Miyamoto, Y.; Rubio, A.; Tomanek, D. *Phys. Rev. Lett.* **2006**, *97*, 126104.

(37) Isborn, C. M.; Li, X.; Tully, J. C. *J. Chem. Phys.* **2007**, *126*, 134307.

(38) Tully, J. C. *J. Chem. Phys.* **1990**, *93*, 1061–1071.

(39) Parandekar, P. V.; Tully, J. C. *J. Chem. Theory Comput.* **2006**, *2*, 229–235.

(40) Desouter-Lecomte, M.; Lorquet, J. C. *J. Chem. Phys.* **1979**, *71*, 4391–4403.

(41) Huber, R.; Moser, J. E.; Gratzel, M.; Wachtveitl, J. *J. Phys. Chem. B* **2002**, *106*, 6994–6999.

(42) Schnadt, J.; Bruhwiler, B. A.; Patthey, L.; O'Shea, J. N.; Sodergren, S.; Odelius, M.; Ahuja, A.; Karis, O.; Bassler, M.; Persson, P.; Siegbahn, H.; Lunell, S.; Martensson, N. *Nature* **2002**, *418*, 620–623.

NL801644D